Tests of first 101 AIT-WATCHMAN PMTs at Boulby

A. C. Ezeribe[1], L. Kneale[1], M. Needham[2], S. Quillin [3], T. Shaw[3], G. D. Smith[2] and B. Wade[2]

[1]Department of Physics and Astronomy, University of Sheffield, Hounsfield Road S3 7RH, UK
[2]School of Physics and Astronomy, University of Edinburgh, Mayfield Road, EH9 3JZ, UK
[3]Atomic Weapons Establishment, Aldermaston, Reading RG7 4PR, UK

September 3, 2020

Abstract

Tests of a pre-series batch of 101 PMTs to be used in the AIT-WATCHMAN experiment are described.

1 Introduction

The photomultiplier tubes (PMTs) are at the heart of the proposed WATCHMAN [1] detector and are critical for its successful operation. The baseline photodetectors for the Inner Detector are 10 inch (253 mm) Hamamatsu R7081 PMTs with low radioactivity glass [2]. Around 3600 PMTs are needed to achieve sufficient photo-detector coverage to meet the non-proliferation goals of the experiment.

To test the suitability of the R7081 a pre-series of tubes was obtained. This note describes the results of the electrical testing of 101 tubes from this batch carried out at the STFC Boulby facility during Autumn 2018. All PMTs were tested in the surface laboratory. A sub-sample of eight tubes were also tested underground. The aims of these tests were:

- To demonstrate that the R7081 meets the requirements of WATCHMAN or a similar anti-neutrino detector and to inform the series production order.
- To gain experience with the operation of the R7081 and prepare for the series production quality assurance and acceptance testing.
- To check that the transportation of the tubes to and operation in the underground laboratory does not affect their performance.

This PMT model is widely used and the results here can be compared with previous experience [3] as well as the shipping data provided by Hamamatsu.

2 Setup

The PMTs were transported to the Boulby site in August 2018 and stored on the surface. Each PMT has an 80 m long cable (BELDEN YR 53485) attached. This supplies the PMT with positive HV and provides the signal return path. An RG59 SHV connector was crimped to each cable prior to testing Boulby [1]. The dimensions of this cable are non-standard and it was necessary the connector pin prior to crimping. More details of this cable and its properties can be found in [4]. The impedance of the cable has been measured to be 50 Ω.

The signal is separated from the high voltage in a splitter box designed by UC Davis (Appendix B). Two boxes were available for these tests: an 8 channel splitter on loan from Davis and a 4 channel box, made to the Davis design at the University of Edinburgh.

A photograph of the setup used for the majority of the tests is shown in Fig. 1. For testing, four PMTs were mounted on a mechanical rig located in a photographers dark tent. Towards the end

[1]Connector type is Radial R317074000.

of the data-taking period a second identical setup was commissioned allowing eight PMTs to be tested in parallel. An additional cloth was draped over the box and the room lights were turned off during measurements. Mounting of the PMTs in the tent required two people due to the restricted space, the need for care when handling the PMTs and the mass of the cable. To mount four PMTs required took around 30 minutes. Fig. 2 shows an electrical block diagram of the setup. A single

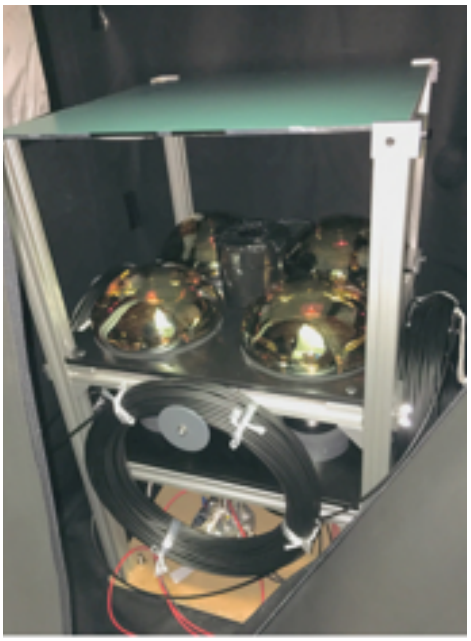

Figure 1: Mechanical rig for the tests at Boulby. Four PMTs are mounted in the rig. The fibre enters the setup from below and illuminates a mirror located around 40 cm above the PMT surface. A blackened barrier prevented direct illumination of the PMTs and supported the neutral density filter.

blue LED with a nominal wavelength of 470 nm provided the light source. The LED driver was triggered at around 10 kHz to allow to produce low intensity pulses of light of $1-2$ ns length. The light from the LED is guided into the dark tent housing the four PMTs under test using an optical fibre. A neutral density filter was used to further attenuate the signal. By reflecting the light from the fibre via a mirror a diffuse source was created that illuminated all four PMTs. This resulted in the PMT signal spectra being dominated by single photoelectron events. The mean number of photo-electrons was measured to be in the range 0.1-0.3. The signal from the PMT was amplified using a commercial fast amplifier (Phillips Scientific PS 775) and the waveforms recorded on a PC using a a CAEN V1730B digitizer. This has 14 bit resolution and a sampling rate of 500 MHz. The digitizer is triggered at 10 kHz via a delayed copy of the LED driver signal. Care was taken to ground the system and shield the signal cables in order to minimize the system noise as much as possible.

The PMTs were placed in the dark tent and left for at least 18 hours under bias voltage before testing to allow the dark count rate to stabilise. The tests were performed at room temperature. This was not monitored during the tests, but seemed to increase substantially during the afternoon when the sun illuminated the window blackout blinds.

For each set of PMTs data was taken to determine the operating voltage needed to achieve a gain of 10^7, the peak-to-valley ratio, the dark count rate and to understand after-pulsing.

3 Waveform Processing

This section describes the procedures used to prepare raw data for live monitoring and online/offline analysis. Table 1 lists details of the five PMT performance characterisation test types. Data were acquired for all of these tests for every PMT at least once. Appendix A contains a table listing all of the PMTs that were tested.

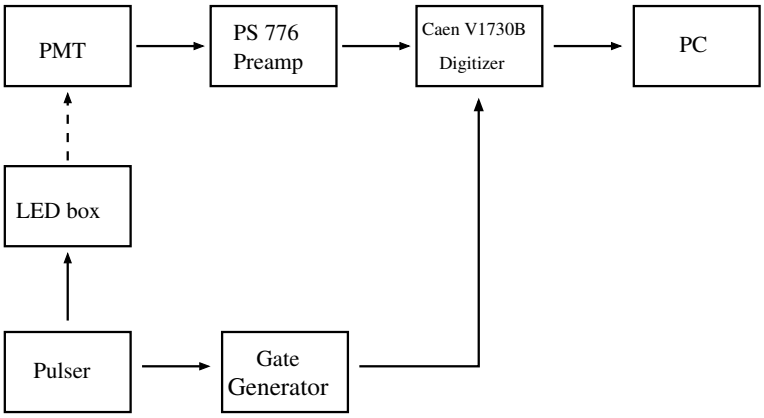

Figure 2: Electronic readout scheme.

	Test Type	ID	Events (M)	Duration (mins)	Gate (ns)	Volume (G)	Description
1	Nominal HV	N	3.0	5.0	220	0.7	SPE at EBB
2	Gain Calibration	G	3.0 x 5	5.0 x 5	220	3.5	SPE at 5 HV steps
3	Operational HV	S	3.0	5.0	220	0.7	SPE at 10^7 gain
4	Afterpulsing	A	0.5	15.0	10200	3.0	SPE at 10^7 gain
5	Dark Counts	D	9.0	15.0	220	2.1	No LED

Table 1: PMT test information. EBB is the manufacturer's HV for 10^7 gain (Nominal HV). SPE refers to data taken using an LED light source with its intensity set to yield a single photo-electron (SPE) level at the PMT photocathode. The digitiser and LED trigger rates were set at 10 kHz for all tests.

3.1 Data Acquisition, Monitoring and Online Processing

Data were recorded as binary files on a Linux PC running CAEN's *wavedump* software. In total around 1.7 T of data were acquired in all 2018 runs. Gain, noise and LED light levels were monitored using histograms of integrated charge. At the time of data taking quantitative information on the mean number of photoelectrons was not available. The light source intensity was therefore monitored (and where appropriate adjusted) by observing the relative contributions of the first and second photoelectron peaks to the charge spectrum. The aim was to just be able to make out the second photoelectron peak on a log-y plot. These charge histograms were also used for *online* gain calibration.

3.2 Offline monitoring and data processing

The data files recorded using *wavedump* were processed using a purpose-made program (BinToRoot[2]) which decoded the raw binary data and created ROOT files containing a TTree and histograms. A canvas of histogram plots was used to monitor data quality and the processing procedure.

Fig.3 shows an example canvas of plots for Test S. The top left histogram is a subset of calibrated waveforms. The accumulation of pulses within a common time interval are due the synchronised LED signal. Evidence of afterpulsing and/or late pulsing can be seen between 100 ns and 180 ns. The blue (red and left hand side blue) vertical lines indicate the signal integration (baseline subtraction) window used to produce the fixed window charge histograms. For each period of data taking with common acquisition settings, the integration windows were set relative to a common LED pulse delay. The delays were found by fitting a Gaussian function to the peak amplitude timing distribution using the **Test S** data. The signal integration window used was 50 ns long starting 15 ns before the mean of the timing peak fit result to ensure the rising edge and tail of the pulses were included, and to accommodate trigger jitter. The width (σ) of the timing

[2] https://github.com/Watchman-PMT/Wavedump_Wrapper/tree/master/Wrapper/BinaryConversion

peak fit was found to be of order 8 ns, consistent with the timing characteristics of the LED, clock jitter and the transition time spread of the LED. This preliminary method of signal integration was developed to accommodate fast bulk data monitoring with a single routine.

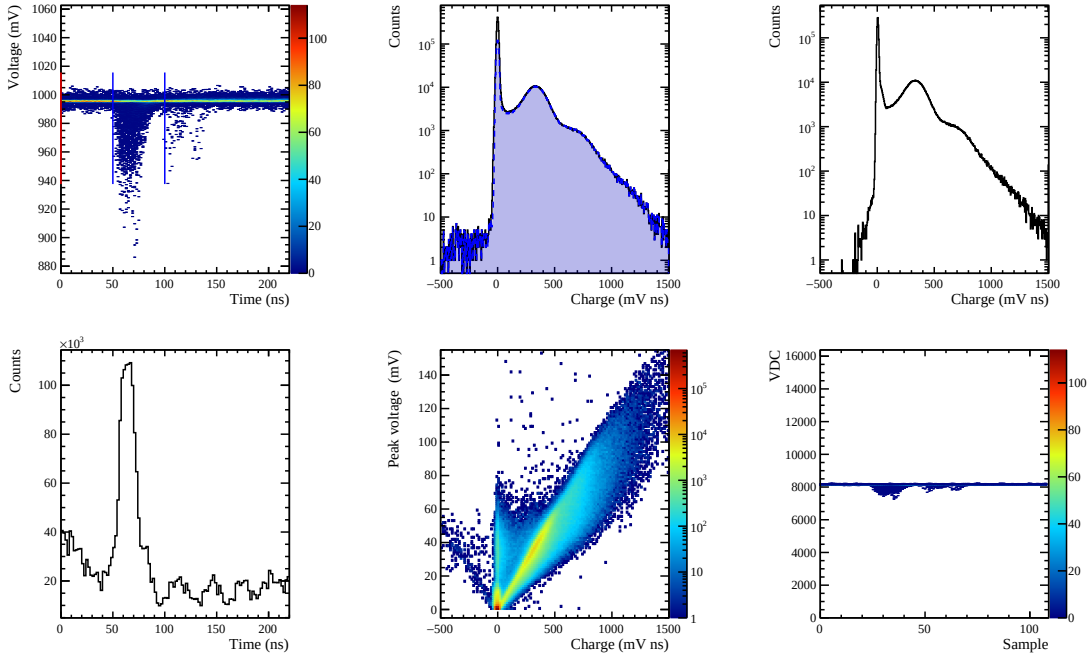

Figure 3: Canvas of plots for Run 2 PMT 132 Test S. Plots are described in the text.

The top middle plot contains two histograms of integrated charge, created using the fixed integration window method described above. In the black solid-line histogram all events were included. In the blue dashed-line histogram a cut was applied to the FFT magnitude to reject (noisy) events with an excess of power at high frequencies; this procedure is described in detail below. Careful inspection of the plot shown indicates that this cut mainly removes events from the pedestal but also some events from the valley region between the pedestal and signal peak.

The top right plot is a histogram of charge created by integrating the signal and baseline regions relative the event-by-event waveform peak; the signal (baseline) region used was -10 ns to 30 ns (-50 ns to -10 ns). The window length used was 10 ns shorter than for the fixed integration window histogram because using the event-by-event pulse peak time cancelled the effects of jitter. In this case events in which the peaks were close to the beginning (<50 ns) or end (>190 ns) of the waveform were rejected leading to around 36 % (80/220) less events with no photoelectron peak present in the signal window. The shoulder on the right of the pedestal has not been investigated in detail but may be due to events in which the waveform peak was caused by noise signals.

The bottom left plot is a histogram of waveform peak time. The large peak at around 65 ns is due to the pulsed LED light source. The count rate rises towards zero due to the first maximum sample in the waveform always being selected.

The bottom middle plot is a histogram of peak voltage versus charge (fixed window method). The baseline was subtracted from the peak voltage using the mean amplitude in the fixed gate baseline integration window. A collection of events for which a linear relationship between peak voltage and integrated charge can be seen as expected. The distribution of points below zero charge are mostly due to dark count signals occurring in the baseline subtraction region and can also be seen below the pedestal in the top middle plot.

The bottom right plot is a subset of uncalibrated waveforms over the full 14 bit digitiser ADC range and for all 110 samples. This plot was used to monitor the baseline and to check for any anomalous signals outside of the standard range.

3.3 Data Processing Output

The histograms of integrated charge and peak time were written to root output files along with a ntuple (root TTree) containing full waveforms and basic analysis variables. The root format allows storage in a compressed and accessible format. A full list of variables are listed in Table 2.

variable name	type	description
`event`	int	event/trigger number
`minVDC`	short	minimum ADC value
`maxVDC`	short	maximum ADC value
`minT`	short	sample number for `minVDC`
`maxT`	short	sample number for `maxVDC`
`peakT_ns`	float	`minT` in ns
`peakV_mV`	float	`minVDC` in mV
`waveform[N]`	short	array of ADC values (N samples)

Table 2: List of ntuple/TTree variables stored in BinToRoot output files.

3.4 Data Quality

The quality of data was monitored throughout data taking with any anomalies noted in an electronic log book. In most cases it was possible to adjust settings (e.g. LED intensity, trigger delay, HV, light-proofing) and re-take data online. Some data quality issues were discovered after the taking data procedure had been completed. These issues are documented below.

3.4.1 Charge Integration Issue

The procedure initially used to integrate charge was found to double count samples at the edges of the integration windows. This led to an overestimation of the gain in the early stages of data-taking. For this reason some data were recorded at operating voltages around 30 V lower than intended.

3.4.2 Noise

After the completion of data-taking, noise signals were discovered in some of the data. It was important to understand and mitigate the effects of this noise to avoid biases to the PMT performance characteristics quantification, and to help reduce noise contributions in future series testing.

An example of a noisy waveform is shown in Fig. 4 (left). The bursts of high amplitude ringing appear at an interval of around 7.5 μs. There are also irregular baseline fluctuations and continuous higher frequency oscillations. These signatures are typical of the noise signals observed, with the noise signal peak amplitudes varying from file to file. The noise power was found to generally be concentrated in specific frequency bands as can be seen from the FFT of the waveform. Most of the power is between 30 and 50 MHz.

Several investigations into the sources of system noise were performed after the completion of pre-series testing. One clear source of noise found is pick-up from USB communications. For the Boulby tests, data transfer from the PC to the digitiser and communications to the HV unit were both done via USB. In the laboratory in Edinburgh it was discovered that communications between the PC and HV card via the VME USB bridge generated high amplitude, radio frequency noise signals in the acquired data similar to that observed at Boulby. The transfer of data from the digitiser to the PC via USB also gave a high rate RF noise pickup. Another source of noise found was due to the (relatively old) pulser used for the tests at Boulby.

The level of noise was also found to be sensitive to the location and design of the HV splitter box. Locating the HV splitter close to rack mounted electronics led to an increase in the noise amplitude. Two HV splitter boxes, made with larger housings yet similar same electrical components, were found to result in higher amplitude noise than a smaller box. The cause for this difference has yet to be identified but presumably is related to the geometrical specifications of the housing and/or length of PCB rails.

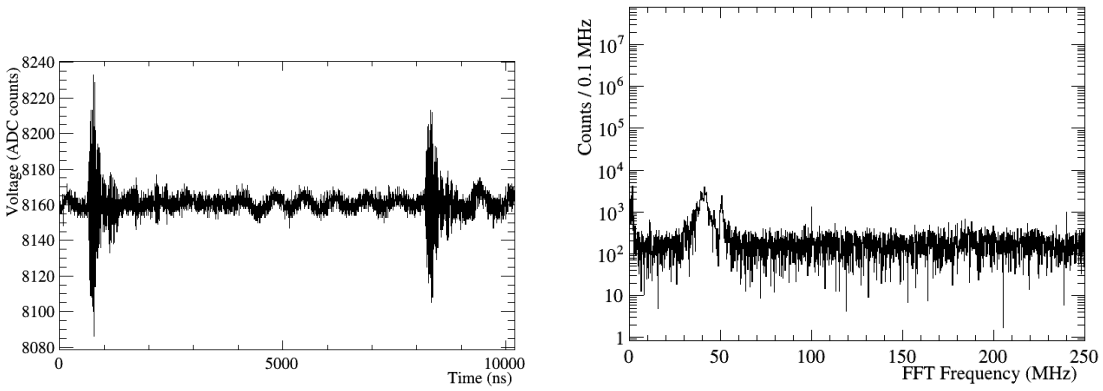

Figure 4: Wavform showing ringing (left) and its Fast Fourier Transform (right). The first (baseline) bin content has been set to zero.

To minimise the contribution of noise to the charge spectra used for offline gain calibration an event vetoing procedure was developed to remove events containing significant levels of noise. This involved applying a selection procedure based on histograms of the waveform FFT magnitude. Each event was only retained if, after zeroing the first (waveform baseline) bin, the bin with maximum number of counts was not in the frequency band corresponding to the observed noise: 40-50 MHz, 100-120 MHz [3].

4 Gain tests

PMT gain is the ratio of the charge output at the anode to the number of photoelectrons produced by conversion at the photocathode. Gain calibration ensures the correct interpretation of the charge output at the PMT anode and is essential in setting operating voltages to achieve a uniform charge response across all PMTs in the detector.

For the purpose of the PMT acceptance testing, the gain tests verify that the required gain can be achieved within the limits of the range of voltages at which the PMT can be operated. The required gain for WATCHMAN is 10^7. The Hamamatsu R7801 can be operated at voltages up to 2000 V. A PMT might be rejected if the required 10^7 gain cannot be achieved below the operating limit of 2000 V, or some specified value below this limit to allow for PMT degradation.

Total gain across the dynode chain varies with the applied voltage V according to equation (1), where a and α are specific to the PMT and n is the number of dynodes in the PMT [5].

$$\text{Gain} = \mathrm{a}^{\mathrm{n}} \left(\frac{\mathrm{V}}{\mathrm{n}}\right)^{\mathrm{n}\alpha} \tag{1}$$

A gain of 10^7 corresponds to a single-photoelectron (SPE) charge output of 400 mVns. The most accurate gain calculation is achieved by fitting the charge distributions produced through integration of the waveforms as discussed in section 3. Characterisation of both the charge response and inherent charge backgrounds of the PMT gives a value for the SPE charge output Q_{SPE}. The gain is then calculated from Q_{SPE} according to

$$\text{Gain} = \frac{\mathrm{Q_{SPE}} \times \text{splitting} \times 10^{-12}}{\mathrm{e} \times \text{amplification} \times \text{impedance}} \tag{2}$$

where amplification = 10, impedance = 50 Ω and splitting = 2, which takes into account the splitting of signal and high voltage from the PMT's single SHV cable.

For the Run 1 and Run 2 tests, each PMT was tested at five voltage values in steps of 100 V in a range around the nominal voltage quoted in the Hamamatsu shipping data to give 10^7 gain. Characterisation of the PMT charge distribution was implemented in stages and the efficacy of

[3] Rejected maximum bins: [8,13], 23, [33,44], [55,∞)

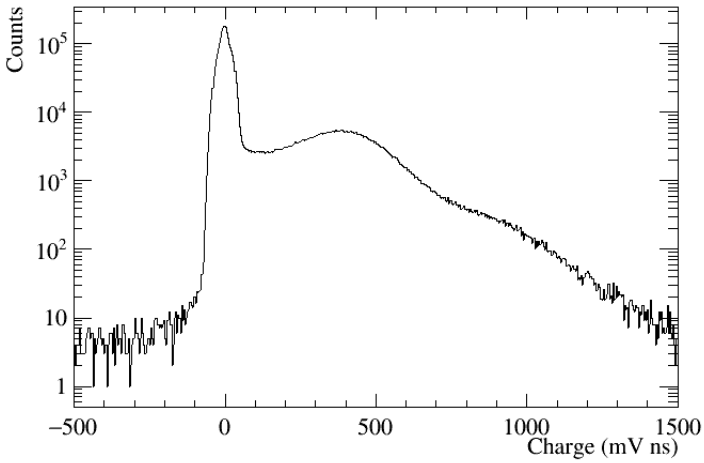

Figure 5: Typical charge spectrum with a pedestal peak at ∼0 mVns, a single-photoelectron peak at ∼400 mVns and later multiple-photoelectron peaks in the tail.

each stage to find the gain at each voltage was compared. The gain data were then fit according to equation (3)

$$\text{Gain} = \left(\frac{\text{V}}{\text{V}_{\text{opt}}}\right)^{\beta} \tag{3}$$

where V_{opt} is the voltage for 10^7 gain and both V_{opt} and β are free parameters in the fit [3]. The *operating voltage* required to give 10^7 gain was then calculated from the fit for each PMT and compared to Hamamatsu's *nominal voltage* for the same gain.

4.1 Characterisation of PMT charge distribution to find the SPE charge output

Features of a typical charge spectrum (Figure 5) can be separated into charge response (signal) and backgrounds. It has a pedestal peak, which consists of the noise inherent in a PMT when there is no signal pulse, a single-photoelectron signal peak and other, multiple-photoelectron signal peaks. A valley region between the pedestal and SPE peaks consists of events due to under-amplified signal and thermionic emission (a source of dark noise) from the photocathode and dynodes [6].

4.1.1 Fit to the signal charge response

The charge response has two contributions: the photoelectric conversion at the photocathode and the amplification at the dynodes.

The photoelectric conversion is the convolution of a Poisson process for the number of photons hitting the PMT and a binary process for the photoelectric conversion. The resulting distribution is Poissonian

$$\text{P}(\text{n}, \mu) = \frac{\mu^{\text{n}} \text{e}^{-\mu}}{\text{n!}} \tag{4}$$

This is the probability that n photoelectrons will be observed when the mean number of photoelectrons collected at the first dynode is μ.

The response of the dynode system is a Poisson distribution but if the amplification is at least 4 per stage (and preferably > 10), then the photoelectron peaks can be approximated with Gaussian functions

$$\text{G}_{\text{n}}(\text{x}) = \sum_{\text{n}=0}^{\infty} \frac{1}{\sigma_{\text{SPE}}\sqrt{2\pi\text{n}}} \exp\left(-\frac{(\text{x} - \text{nQ}_{\text{SPE}})^2}{2\text{n}\sigma_{\text{SPE}}^2}\right) \tag{5}$$

where σ_{SPE} is the width of the SPE distribution, x is the charge variable and Q_{SPE} is the SPE charge output.

Where the amplification is low, which can be the case particularly at the first dynode when the number of photoelectrons is only 1 or 2, the Gaussian approximation does not hold and the single and multiple-photoelectron Gaussians should be replaced with sums of Gaussians (6),

$$G_n(x) = \sum_{m=0}^{\infty} \frac{(n\frac{Q_{SPE}}{Q_{SPE,2}})^m e^{-n\frac{Q_{SPE}}{Q_{SPE,2}}}}{m!} \frac{1}{\sigma_{SPE,2}\sqrt{2\pi n}} \exp\left(-\frac{(x - mQ_{SPE,2})^2}{2m\sigma_{SPE,2}^2}\right) \tag{6}$$

where m is the number of electrons produced at the first dynode, $Q_{SPE,2}$ is the charge output by a single electron emitted from the first dynode and $\sigma_{SPE,2}$ is the width of the distribution in the Gaussian approximation.

The ideal PMT response is then a convolution of the capture & photoelectric conversion with the amplification (7).

$$S_{ideal}(x) = \sum_{n} P(n, \mu) G_n(x) \tag{7}$$

4.1.2 Fit to the backgrounds in the charge distribution

There are two types of background. The low-charge processes which occur when no photoelectron is emitted from the photocathode give rise to the pedestal, which has a Gaussian distribution. The processes which can accompany the signal e.g. spontaneous emission from the photocathode and dynodes give rise to the valley. These can be approximated by an exponential. The backgrounds are the sum of these processes (8).

$$B(x) = P(0, \mu) \frac{1}{\sigma_0\sqrt{2\pi}} \exp\left(-\frac{x^2}{2\sigma_0^2}\right) + P_{exp}\theta(x)\alpha \exp(-\alpha x) \tag{8}$$

where $P(0, \mu)$ is the Poisson probability that 0 photoelectrons are produced, σ_0 is the width of the pedestal, P_{exp} is the probability that the second type of background is present and α is the coefficient of the exponential decrease of the valley. $\theta = \begin{cases} 0 & x \leq 0 \\ 1 & x > 0 \end{cases}$ ensures that there is an exponential component only if $x > 0$.

4.1.3 Fit to the total charge spectrum

The total charge distribution can therefore be modelled according to equation (9).

$$Q(x) = P(0, \mu) G(x)_{ped} + P_{exp} Exp_{val} + \sum_{n=0}^{\infty} P_n G(x)_n \tag{9}$$

where G_{ped} and G_n are the Gaussian fits to the pedestal and n-photoelectron peaks, the Poisson distributions give the relative fractions of each peak and Exp_{val} is the exponential fit to the valley.

4.2 Gain calibration procedures

Knowledge of the operating voltage to achieve 10^7 gain was needed online during data taking. Since the fit was still being developed and not yet stable, this was done by taking the position of the maximum in the SPE-peak range minus the position of the maximum in the pedestal-peak range. The full fit model according to equation (9), with double-Gaussian fit to the pedestal, Gaussian approximation to the single- and double-photoelectron peaks and exponential approximation to the valley generally resulted in a precise fit (Figure 6) to the pedestal and SPE peaks, which are key in the calculation of the SPE charge and thus in the operating voltage determination.

The length and timing of the waveforms was found to depend on the applied voltage such that pulses arrived sooner and lasted for longer at higher applied voltages. The former effect is consistent with the expectation from the datasheet that the transit time decreases by around 12ns from 1300 V to 200 V. To ensure all the charge is collected for all runs, an integration window of 70 ns was found to be needed. Fits were further improved by applying an FFT noise filter to the waveforms when producing the charge spectra (section 3.4). Figure 6 shows a typical fit to the SPE distribution and a typical fit of several voltages to extract the gain.

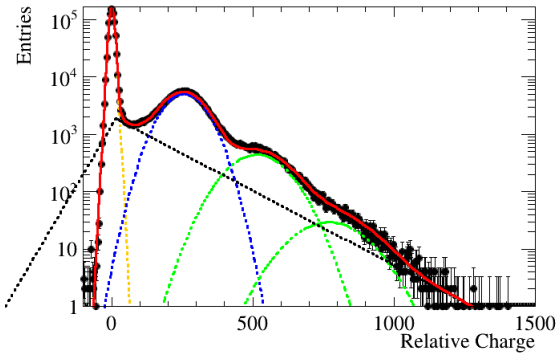

(a) Fit to charge spectrum.

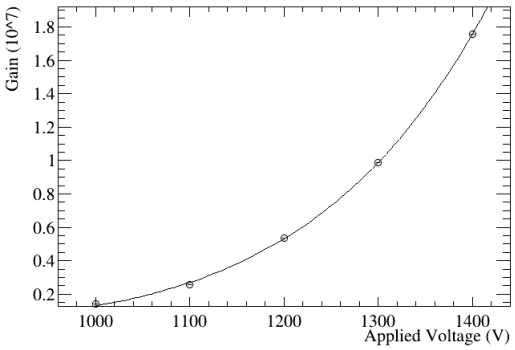

(b) Fit to gain curve.

Figure 6: Results based on full fit with double-Gaussian fit to the pedestal (yellow), Gaussian approximations to single- (blue), double- and triple-photoelectron (green) peaks and exponential approximation (black) to the valley.

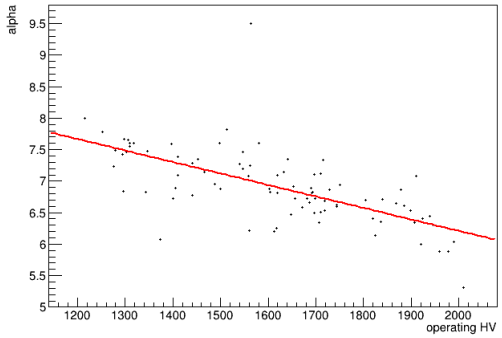

Figure 7: Value of alpha from the fit as a function of operating voltage calculated.

The value of α in equation (1) is dependent on the gain and the voltage applied. The mean value of alpha was found to be 6.9, which agrees with a value of approximately 0.7 per stage. Figure **??** shows the alpha values as a function of operating voltage for 86 of the tested PMTs.

The results obtained are correlated with the Hamamatsu datasheet though with a $\sim$ 30 V offset (Figure 8). This may be the result of signal attenuation in the 80 m cable, such that higher operating voltages are required to achieve the desired output. It is understood that the Hamamatsu tests were carried out without cables.

4.3 Gain test outcomes

A relatively robust and automated fitting regime was developed for the gain calibration. Difficulties arise due to the large variation in the spectra over the voltage range. Possible improvements are being investigated. First, the choice of voltage scan points could be improved to be better centered

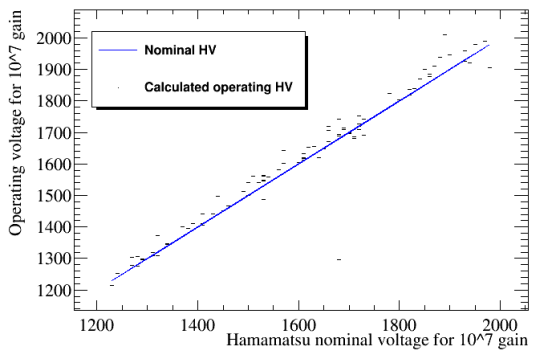

Figure 8: Comparison of calculated operating voltages with Hamamatsu nominal voltages for 10^7 gain from full fits to filtered histograms. The outlier is PMT 160, which has been put down to an error in the shipping data.

on the operating voltage. Further work is needed on the initialization of the fit to improve the robustness. Incorporating a sum-of-Gaussians fit to the SPE peak into the full fit model may improve the fit to the tails of the spectra. An alternative fit to the valley with a Γ function rather than exponential will also be investigated.

Further refinement of the spectral plots including refinement of the noise filtering is likely to improve the robustness of the fitting for gain calibration, as will noise reduction in the experimental setup for future tests. With the exception of a single PMT, all PMTs achieved 10^7 gain at close to the Hamamatsu nominal voltage. However, the operating voltages calculated are offset by ~ 30 V higher than the Hamamatsu nominal voltages quoted on the datasheet. This could be due to the cable. All PMTs were found to achieve 10^7 gain at less than 2000 V. For those PMTs requiring close to the 2000 V limit for 10^7 gain, long-term investigations into the extent and timescale of gain deterioration are planned.

5 Peak to valley

The peak-to-valley, the ratio of the height of the single-photon peak to the minimum of the charge spectrum characterises the signal-to-noise performance of the PMT. It can be extracted in two ways, either by fitting the full charge spectrum or by making local fits to the relevant regions. This section describes a study using the second method. For this method to be valid the light-level should be low enough to ensure the location of the single photon peak and the maximum of the charge spectrum coincide. This study is made using the data taken at the working voltage which gives 10^7 gain.

The method works as follows. The **ROOT** class **TSpectrum** is used to identify the location of the pedestal and signal peaks. Based upon the results of this a local fit of a parabola (Gaussian) is made to the valley (signal) regions respectively. Once the location of the minimum and maximum are identified it is straightforward to calculate the peak-to-valley. The uncertainty of the procedure from propagating the uncertainties on the fitted parameters reported by **Minuit** is 0.01. For some PMTs repeated datasets were taken in identical conditions. From these data the uncertainty on the peak-to-valley is estimated to be 0.01-0.02, in agreement with the **Minuit** estimate.

Fig. 9 shows the peak-to-valley ratio determined by this method, using the fixed window method to calculate the SPE, compared to the value provided on the Hamamatsu datasheet. Though there is a clear correlation between the measured peak-to-valley and the expectation from Hammatsu datasheet, the measured values are clearly smaller. For a few PMTs the peak-to-valley falls below 2, which might be considered as a reasonable criteria for rejection. Insight into the worse peak-to-valley can be gained by dividing the data according to the location of the PMT in the first mechanical rig (Fig. 10), which was used for the majority of the data taking. For positions 1 and 3 in Rig 1 there is better agreement with the Hammatsu datasheet. This suggests that the worse performance compared to the datasheet isrelated to the setup and not the PMTs themselves. Possible causes are differences in illumination between the PMTs or variations in the system noise with PMT location (Section 3.4). It is difficult to quantify the exact impact of these effects on the peak-to-valley ratio itself but suggests that for the long term effect better control of both is needed. Comparisions have also been made of the peak-to-valley on the surface and underground. Good consistancy is found between the measurements, with some hint the performance is better underground, perhaps due to reduced electromagnetic pickup.

6 Dark count

6.1 PMT Dark Rate Measurements

Dark count test data was acquired by triggering the digitiser for 15 minutes at 10 kHz with a record length of 110 samples at 2 ns per sample in the absence of a light pulse. This gave a nominal 9×10^6 records with a total testing time of 1.98 s per tube. Dark noise pulses were identified and counted during post process analysis of the saved data. The testing procedure ensured that the tubes were biased at the nominal operating voltage in the dark tent for at least 18 hours prior to acquiring the dark rate data. The PMT power supply for each tube was set to the operating voltage calculated from the gain test data at the time of testing. This is not necessarily the value that would be calculated from a considered analysis subsequently. However, the dark rate is not expected to be strongly dependant on operating voltage.

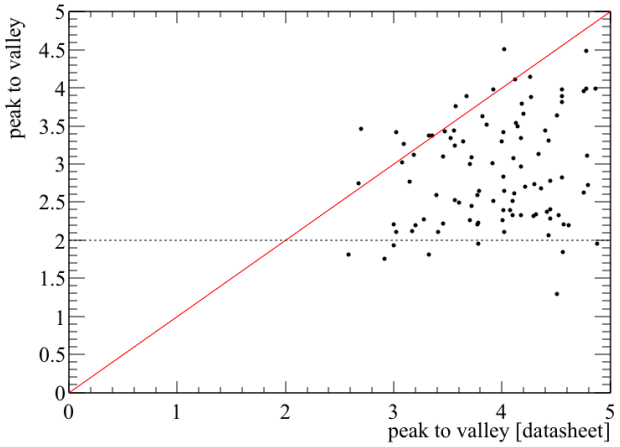

Figure 9: Measured peak-to-valley measurements, measured on the surface, versus the Hamamatsu datasheet values.

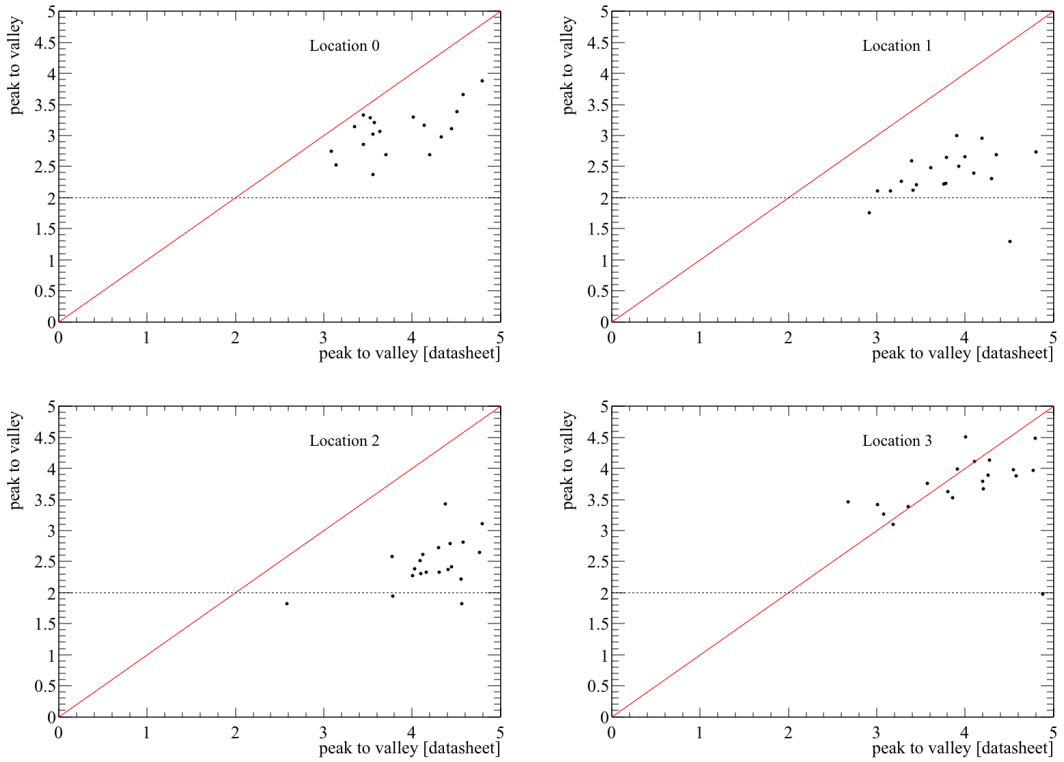

Figure 10: Measured peak-to-valley measurements, measured on the surface, divided in to locations of the PMTs in Rig 1, versus the Hamamatsu datasheet values.

A dark pulse was deemed to have occurred if a 220 ns record contained a signal level exceeding a set threshold. The probability of multiple true dark pulses in a single record was assumed to be negligible. Multiple pulses were treated as double-pulsing phenomena and a maximum of one dark pulse per record was counted. No check on the pulse shape, duration or integrated charge was made to confirm that a genuine dark event had occurred.

The method used by Hamamatsu is unknown. The R7081 PMT data sheet Ref [2] quotes a typical dark count after 24 hours storage in darkness of 8,000 s^{-1} at LLD: 1/4 p.e. This is presumed to mean that a lower level discriminator is set to a threshold equivalent to one quarter

of the mean single photo-electron (PE) signal amplitude. Hamamatsu data sheet characteristics are quoted at 25° C. At the time of the measurements, the acceptance criterion was that the dark count rate should be less than 10,000 s^{-1}.

6.2 Method

The dark rate was calculated by making a histogram of the maximum signal value recorded in each record known as a Pulse Height Distribution (PHD), and counting the number of entries above a suitable threshold. A threshold derived from the value of the SPE charge integral mean signal level,

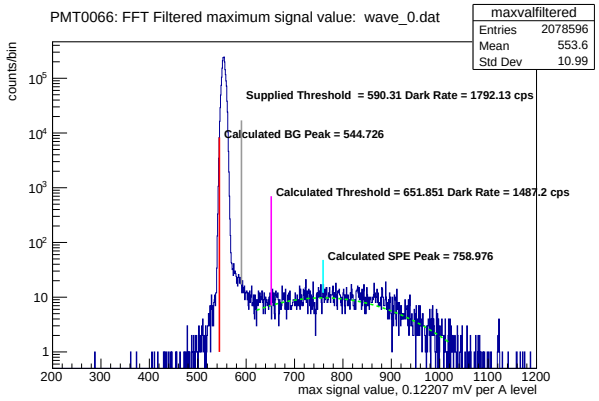

Figure 11: Example Pulse Height Distribution showing threshold selection.

to compare with the Hamamatsu measurements, would best be calculated from measurements of gain where the PMT is illuminated. Such data was not available at the time of the initial dark count rate analysis and a number of methods to determine a threshold without external information were attempted. The noise issue discussed in Section 6.5 complicated internal automatic threshold determination and a manual, subjective identification of a valley location beyond the pedestal for each tube PHD was used for the dark count rate analysis. All data was filtered by the Fourier spectrum cut outlined in Section 6.5 before the PHDs were constructed. A PHD example is plotted in Figure 11. The horizontal axis shows the maximum signal in units of digitiser Analogue to Digital Converter (ADC) value. One ADC unit is calculated to be the equivalent of 0.12207 mV. The red vertical line marks the location of the background signal calculated from the mean value of all records. Dark rates estimated from a number of threshold location methods are shown. The cyan line shows the peak of a Gaussian fit to the data above the pedestal (in excess of 600 ADC units) assuming this to be an estimate of the SPE peak. The pink line shows the position of a threshold halfway between the baseline and the peak fit maximum giving a dark rate of 1487 Hz. The grey line shows the position of a threshold estimated from the integrated charge as shown in Section 6.6 giving a dark rate of 1792 Hz. The manual threshold location for tube #0066 was ADC channel 630 and gave a dark rate of 1686 Hz.

6.3 Results

The distribution of dark rates for the 101 tube sample measured at the Boulby above ground lab (RUN000001) is shown in Figure 12(a). Thresholds for these measurements were set manually to a suitable valley location in the PHD. The dark count rate for each tube is plotted against results included in the Hamamatsu shipping data in Figure 12(b). All tubes showed dark rates below the 10 kHz acceptance criterion and had a mean value around 2.5 kHz. Some correlation with the Hamamatsu data is apparent though there are outliers in both directions.

6.4 Dark Rate Temperature Sensitivity

The dark count rate is expected to be dominated by thermionic emission and as such is strongly dependant on absolute temperature [7]. Figure 13 plots the dark rate for an R7081 tube measured in a temperature controlled environment at Edinburgh University during the Spring of 2019. The

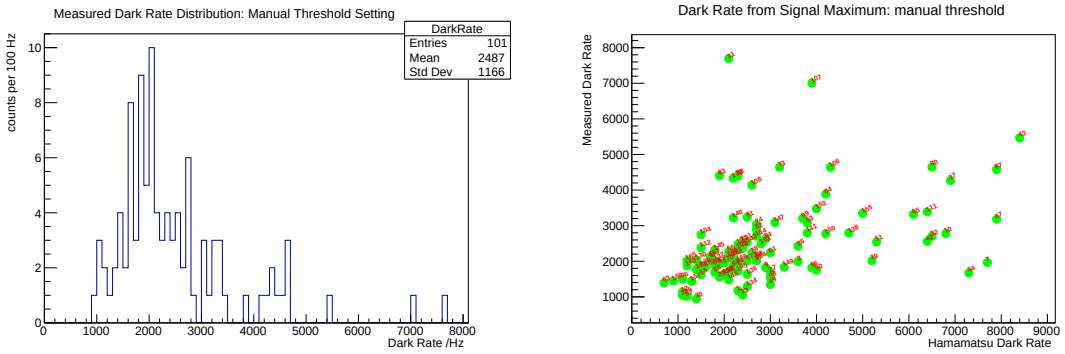

(a) Measured Dark Rate for the 101 PMT tube tests

(b) Measured Dark Rate versus Hamamatsu Shipping Data

Figure 12: Distribution of results for RUN000001.

plot suggests a temperature sensitivity of ∼60 HzK^{-1} or 7% at 20 °C and ∼150 HzK^{-1} or 12% at 25 °C. These values are consistent with the value of 100 HzK^{-1} at 20 °C reported by the Double Chooz experiment [3] and in literature [8].

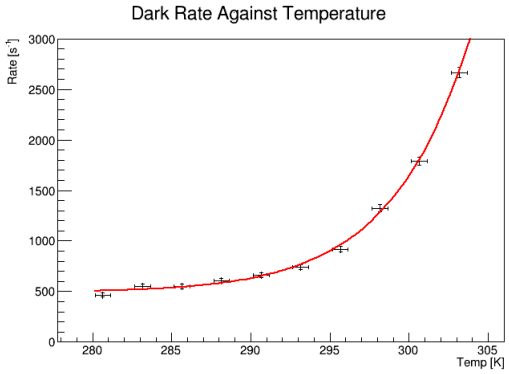

Figure 13: Dark rate versus temperature for an R7081 tube.

Temperature of the PMTs was not controlled nor monitored during the testing. The laboratory temperature was felt subjectively to increase substantially during afternoons when the sun warmed the window blackout blinds. Additionally, a supply voltage of 1500 V would mean that each tube generated ∼ 180 mW in the 12.7 MΩ resistor chain leading to a potential maximum temperature increase of ∼0.6 K per hour assuming 1400 g of glass with a heat capacity of 0.83 $kJkg^{-1}K^{-1}$. The uncertainty in tube temperature during testing needs be considered when comparing measured dark rate data to manufacturers data or to requirements. Better monitoring and control of PMT temperature will be implemented for future acceptance testing.

6.5 Dark Rate Noise Issue

The noise issue described in Section **??** initially became apparent from inspection of dark rate data PHDs. Some histograms had pedestal shapes that appeared much wider than others. Figure 14 shows a comparison of a clean and a noisy example. Inspection of data suggested an intermittent ringing noise that when present affected all 4 channels simultaneously (8 in the two tent setup) as shown in Figure 15. Noise appeared in the data recorded from both the above and underground laboratories, possibly indicating a source within the experimental setup.

An example of a PMT pulse unaffected by noise and it's Fourier transform is shown in Figure 16. The frequency spectrum has the highest powers in the lowest non-zero bin and can be contrasted with the noisy spectra shown in Figure 15. A example plot of the peak signal value against the peak FFT output bin for a noisy data set is shown in Figure 17. The FFT power can be seen in specific frequency bins.

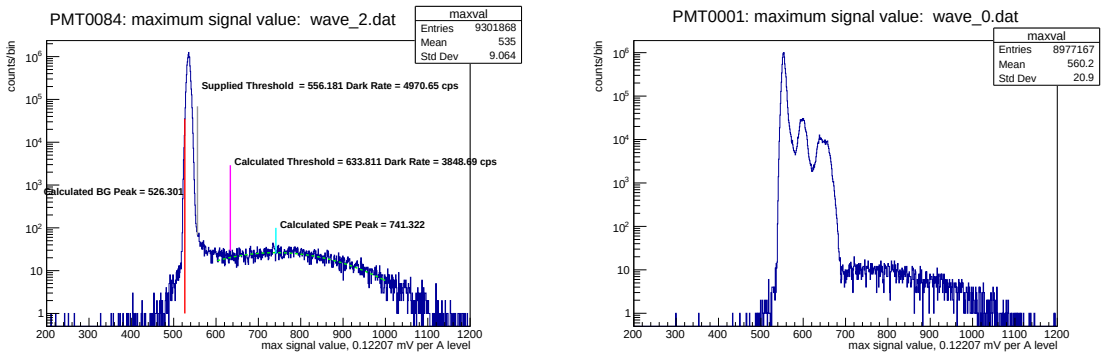

(a) Clean Data. (b) Noisy Data.

Figure 14: Comparison of data sets less and more affected by noise.

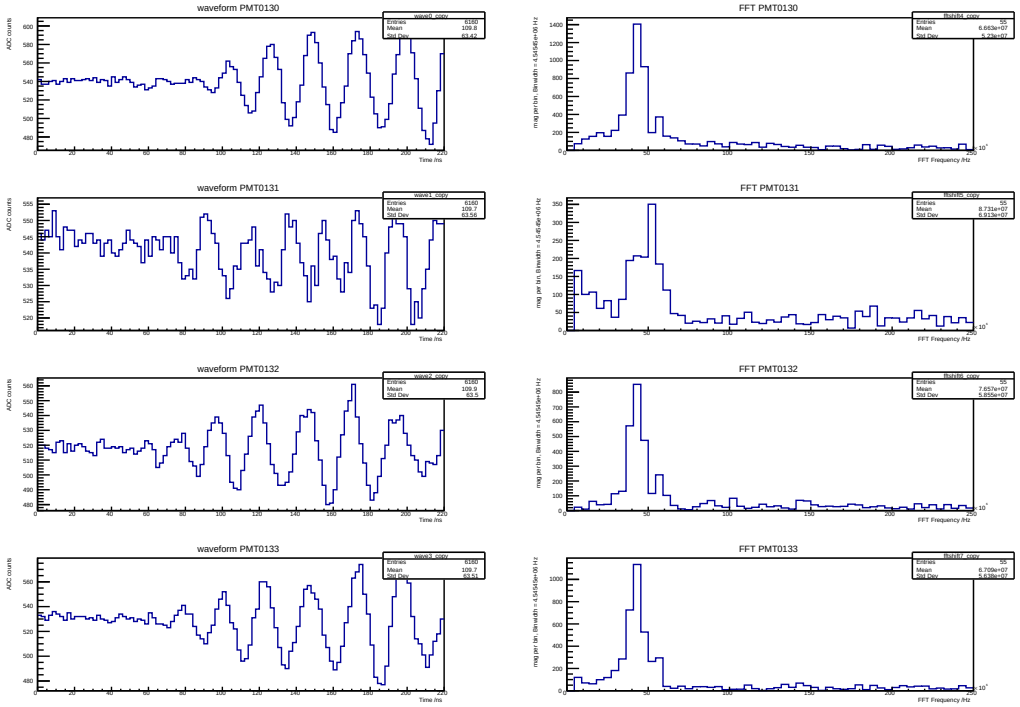

Figure 15: A single noise pulse recorded simultaneously on four PMTs. Fourier transforms of the traces are shown in the right hand plots.

A simple filter based on the frequency spectrum of each record was used to reject any records with a peak power not in the lowest non-zero bin. The results of applying this cut to a noisy data set is shown in Figure 18. The number of records passing the cut for this data set was 2,409,705 from the original 8,594,099. Use of the FFT cut enables a dark count rate to be made that would otherwise have been difficult or impossible. Note that the effect of the effective acquisition time of cutting records with signals above the threshold is ignored.

6.6 Dark Rate Data Charge Integral Measurements

The charge integral distribution was measured from the dark rate data for all PMTs. Such measurements are less satisfactory than the illuminated gain test data due to the lower data rate, only 4,000 dark pulses might be expected during a 2 second acquisition. Additionally, the random time of arrival of pulses within the acquisition window means that some are too close to the window boundaries to be analysed.

It was not possible to use analysis methods developed for the illuminated gain measurement

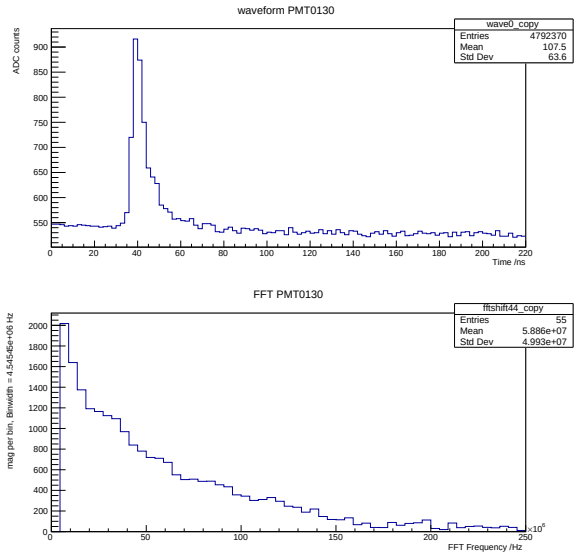

Figure 16: Example of a PMT pulse unaffected by noise and its Fourier transform.

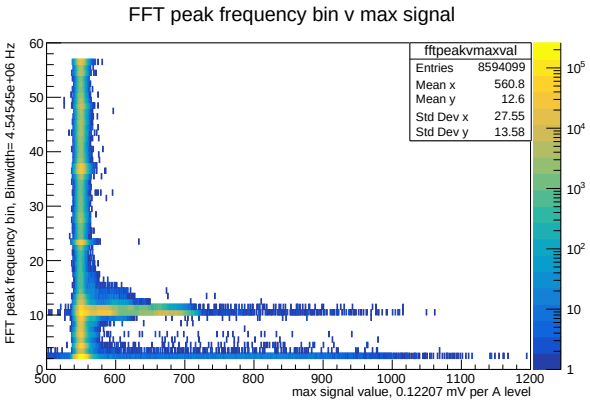

Figure 17: Plot of the highest power FFT bin against the maximum signal value for a noisy data set. Horizontal bars show the presence of noise at fixed frequencies.

data as the peak signal value could appear randomly within the acquisition time window rather than close to a defined trigger point. Suitable peaks were located via the **ROOT TSpectrum** method. Only records with single peaks were selected for charge integral determination. Peaks were also required to be within the time range 10 ns to 170 ns in the 220 ns window to ensure that it was possible to fully bracket the complete signal. The integration window used was 48 ns long (or 24 bins) in total with 5 bins (10 ns) before 19 bins (38 ns) after the peak bin location. To simplify the calculation and remove the need to determine the background value for each data trace (possible further reducing the number of suitable traces) the background value was taken as the mean of the Fast Fourier Transform (FFT) zero bins for all data traces. This is equivalent to the mean data trace offset.

Figure 19 shows an example charge integration histogram from dark rate data. Figure 20 shows the correlation of maximum signal value with the charge integral and how a threshold value for the dark rate measurement may be calculated. The mean integrated charge value for the 101 PMTs is shown in figure 21. Data is from the above ground RUN000001 data only. Values are consistently less than the expected 400 mVns. Subsequent analysis of the gain data suggests that a longer integration window results in a higher gain i.e. that the current analysis might underestimate the charge integral.

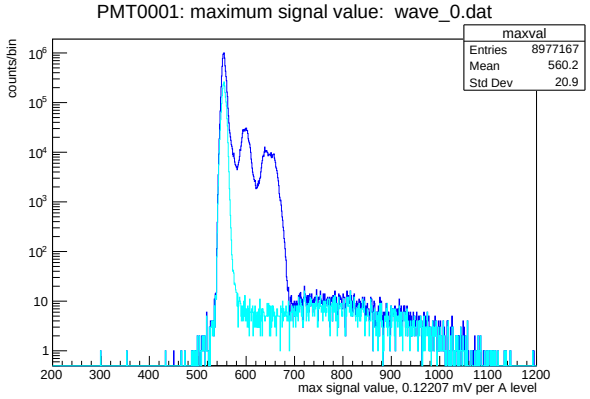

Figure 18: Effect of the simple FFT filter on a dark rate PHD. The cyan trace shows the effect of the cut.

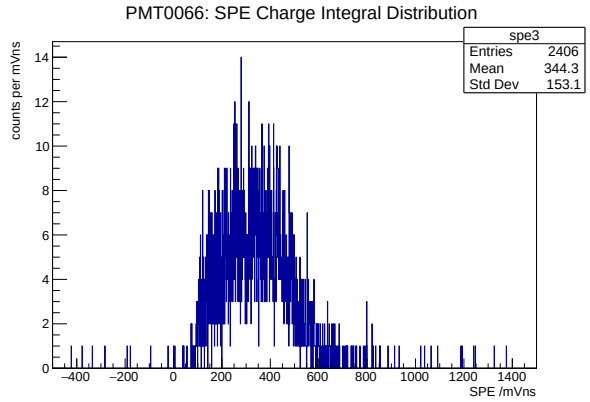

Figure 19: Example Charge Integral distribution for dark rate data

6.7 Underground Measurements

Subsequent to the main data taking exercise, testing all 101 PMTs above ground in RUN00001, a number of smaller scale tests were made to look for potential effects of moving the PMTs to the underground laboratory and operating them there. Measurement of dark count rate from these runs showed large fluctuations. It is thought that the limited time available for equipment setup, temperature variations and possible light leakage may have affected the results and that conclusions on the effects of underground operation cannot be drawn.

7 After-Pulsing and Late-Pulsing

To extract single photo-electron signals from data, any unwanted secondary signal present in the data should be understood and accounted for in analyses. The major cause of these secondary signals is after-pulsing due to electrons that scatter inelastically off the first dynode [9, 10]. Also, ions produced during electron collisions with residual gas nuclei in the PMT cause late-pulsing. These late-pulsing signals are expected to arrive the PMT anode outside the LED gate without any preceding LED signal. In this analyses, only secondary charge signals that arrived the PMT anode after the time window of the main LED signal were considered. As shown in Table 1, a readout gate (charge digitization window) of 10.2 µs was used while collecting these after-pulsing data set.

Charge signal candidates were categorised into Double-pulses (DP), Fast after-pulses (FAP), Late after-pulses (LAP), Very-late after-pulses (VLAP) and Late-pulses (LP) based on their temporal separation relative to the main LED charge signal as shown in Figure 22.

As shown in Figure 22a, after-pulsing hits with a temporal separation of $\leq$100 ns (>100 ns to $\leq$1 µs) that are preceded by a main LED hit are Double-pulses (Fast after-pulses). Here, a hit is

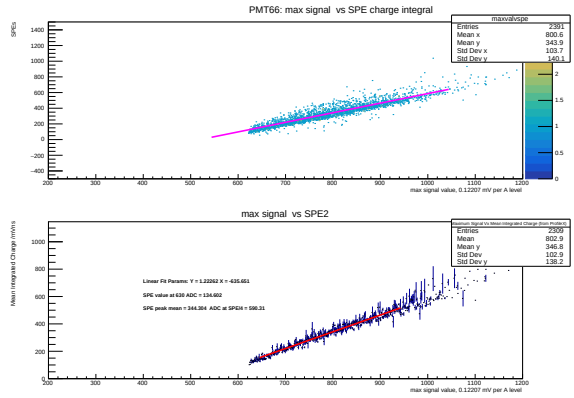

Figure 20: Plots showing correlation of maximum signal value with the charge integral.

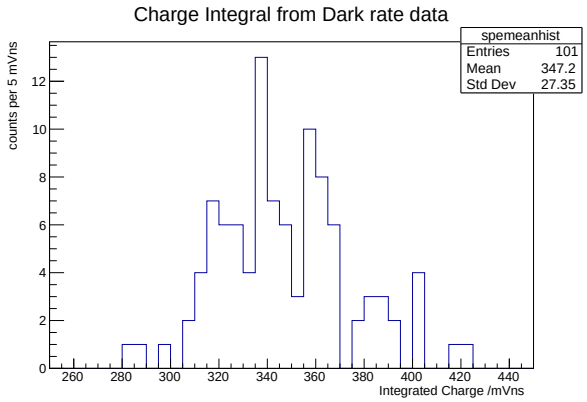

Figure 21: Distribution of charge integrals from RUN000001 dark rate data.

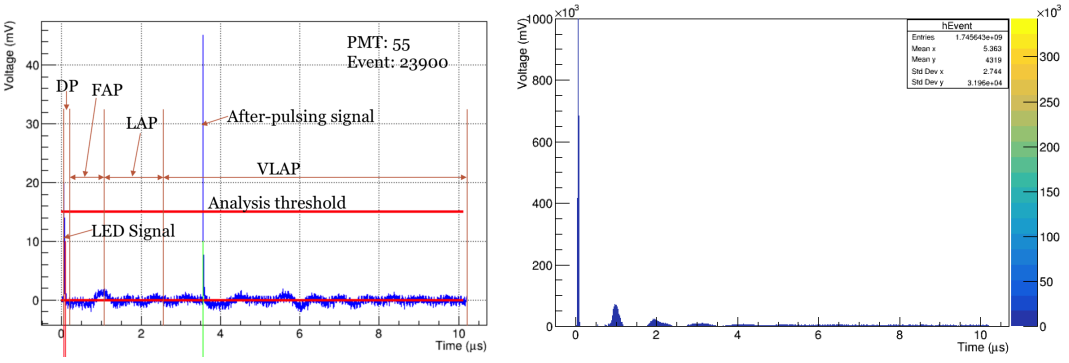

(a) Single after-pulsing signal.

(b) Distribution of after-pulsing and late-pulsing signals.

Figure 22: Sample of an event showing the DP, FAP, LAP and VLAP regions in (a). In (b) is combined after-pulsing and late-pulsing events obtained from all the 100 PMTs.

PMT charge signal with an amplitude of >15 mV. Late after-pulses (Very-late after-pulses) were required to have a temporal separation of >1 µs to ≤2.5 µs (>2.5 µs) from the main LED hit. Any PMT hits without a prevenient LED hit was analysed as a Late-pulsing. Counting from 0, the first peak in Figure 22b is the LED signal while the second and the 3rd peaks are in the FAP and LAP regions.

Data digitization offset was corrected on event-by-event basis using the average of the first 20 ns data before the arrival of the main LED signal 60 ns later. Results of this baseline correction

method can be seen in figure 22.

7.1 After-Pulsing and Late-Pulsing Probabilities

The probability P of after-pulsing or late-pulsing occurring in a given PMT was computed using:

$$P = \frac{100 \times n}{N}\,, \tag{10}$$

where n is the number of the after-pulsing or late-pulsing events in a total number of N events.

For stability checks, a set of 12 PMTs were tested more than once using the rig shown in Figure 1 in a set of 4 PMTs or 8 PMTs (if the second test rig was used). Results from these PMT stability tests are shown in Figure 23. The lab temperature during these tests was in the range of 20 °C to 22 °C. PMT characteristics such as anode currents can vary with operating conditions which includes the lab temperature. As shown in Figure 23a, the P parameter for Run1 are in the range of 1.4% to 2.4% for the LP and <0.6% for DP, FAP, LAP and VLAP. Integral charge signal in the after-pulsing were found to be in the range of 18% to 37% of the main LED signal, see Figure 23b. This is the percentage of the charge integral for signals above the analysis threshold in the after-pulsing and LED gate. It can be seen in Figure 23b, that only 5% to 15% of the N events have signals in the LED gate. This implies that about 85% of the triggers occurred outside the LED signal time or it occurred with an LED signal that is below the analysis threshold. The P parameter for the LP as obtained from Run2 (for the same set of PMTs used in Run1) are in the range of 1.9% to 2.8% while the DP, FAP, LAP and VLAP results are <0.6%, see Figure 23c. Figure 23d shows that the integral charge in the after-pulsing for Run2 are between 19% and 39% while 5% to 24% of all the events had LED signals. These Run2 results are consistent with the Run1 results. A subset (4 out of 8) of the PMTs tested in Run1 and Run2 were used in Run3. The P parameter for the LP events were between 3.6% and 6.9% and that of the DP, FAP, LAP and VLAP were <1.2%, see Figure 23e. The integral charge in the after-pulsing signals were found to be between 46% and 54% in Figure 23f relative to the LED signal. These Run3 results are a factor of 2, in average, larger than results from Run1 and Run2. This could be due to contributions from difference in the LED intensity during the tests as However, the number of the events with LED signal of 10% to 21% from Run3 is consistent with results from both Run1 and Run2. The P results for LPs in Run4 was found to be between 1.7% and 3.7% while that of DP, FAP, LAP and VLAP were <0.4% as shown in Figure 23g. The charge in the after-pulsing signals were between 51% and 63% while 8% to 12% of pulses had LED event in the main signal gate, see Figure 23h. The distribution of the after-pulsing and late-pulsing amplitude in these tests peak at 33±6 mV.

These P results from the R7081 PMTs are consistent with results in Ref. [11] obtained from R7525 PMTs. However, the Double Chooz experiment reported a P parameter of 10%±5.4% for the R7081 PMTs over a longer gate of 0.1 µs to 16 µs in Ref. [12] relative to an average of 1.5% observed in this measurement over a gate of about 0.09 µs to 10.2 µs. Note that systematic uncertainties were not accounted for in the results of Ref. [12].

8 Summary

In this note results of series testing of 101 PMTs at Boubly has been presented. The tight timescale for the tests created considerable challenges, in particular related to understanding system noise. Despite this all the PMTs were tested and the PMT characteristics verified against the Hammatsu datasheet. In particular:

- All PMTs were functional and worked after transportation from Japan to the United States and then to Boulby.
- A subset of PMTs were successfully transported underground and tested. No significant difference was found in PMT behaviour between the surface and underground tests.
- The operating voltage was found to agree with Hammatsu at the level of 20 V. Given that Hammatsu made measurements of the bare PMT prior to connecting the cable this agreement seems reasonable.

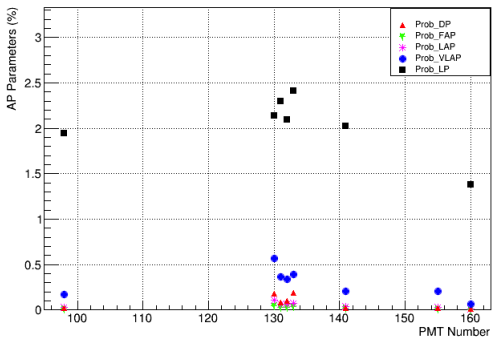

(a) AP and LP probabilities from R1.

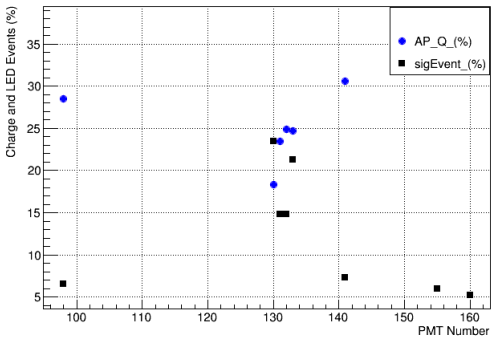

(b) % AP charge and LED events from R1.

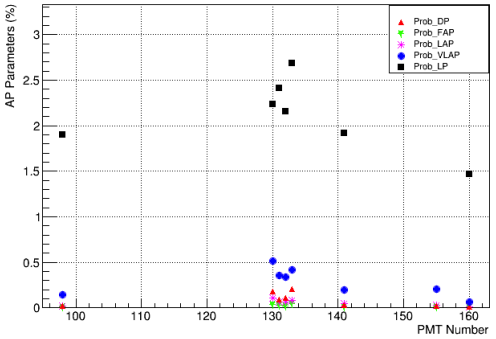

(c) AP and LP probabilities from R2.

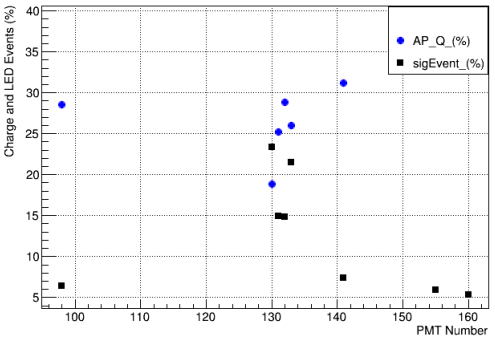

(d) % AP charge and LED events from R2.

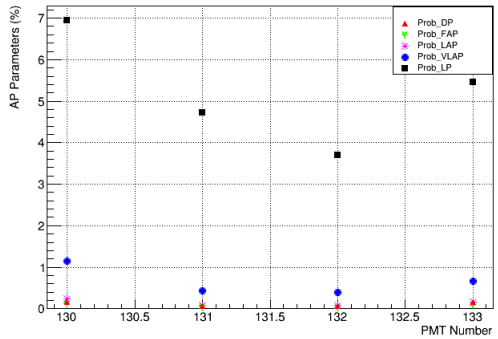

(e) AP and LP probabilities From R3.

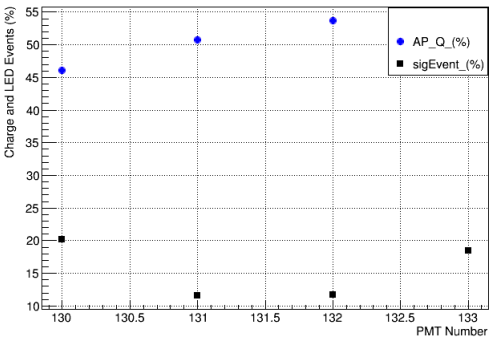

(f) % AP charge and LED events from R3.

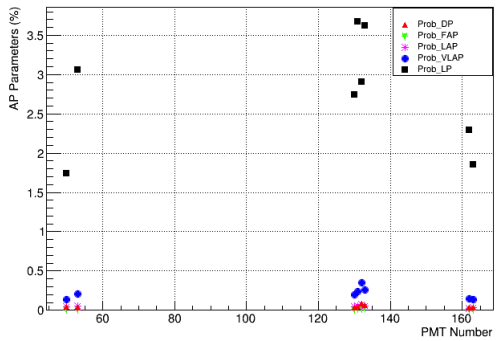

(g) AP and LP probabilities from R4.

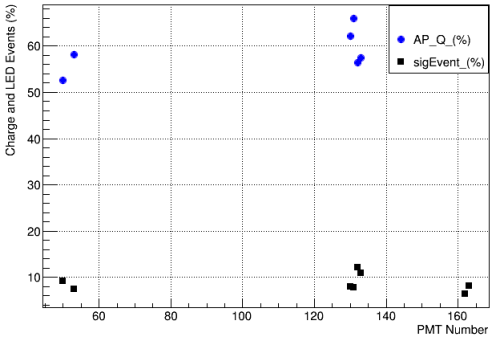

(h) % AP charge and LED events R4.

Figure 23: PMT performance stability test results. Here, "Prob" label represents P as defined in Equation 10 and DP, FAP, LAP, VLAP and LP are as defined in the text. AP stands for after-pulsing. R1 - R4 represent Run1 - Run4.

- Measurements of the peak-to-valley and dark count rate were clearly affected by the system noise. Allowing for this qualitative agreement is found with the Hammatsu measurements. For the final series testing better control of the system noise is needed but it is unlikely any PMT tested would be rejected based on either their peak-to-valley or dark count performance.

- Measurements of the after-pulsing rate are consistent with previous tests of these tubes made by other groups [12].

Considerable experience was gained in operating these tubes which will be invaluable for the series testing rigs which are being constructed in Edinburgh. In particular several sources of system noise have been identified. Care is needed with USB data transfer as it can inject high frequency noise into the system. For the long-term test setups the digitized waveforms will be transfered via an optical link rather than the VME bridge. The control of the HV cards will still be via USB. However, laboratory tests indicate that high frequency noise from this source can be almost eliminated using a USB isolator and attaching ferrite beads to the USB cables. A new pulser has been purchased and this seems to be cleaner in noise performance compared to the old pulser. For the final system better care has been taken in terms of running of cables and grounding of the system. Ferrite beads have also been attached to all power leads. These improvements have led to a system with considerably better noise performance than those for the the pre-series tests. The only remaining issue to be understood is that of the design of the splitter box.

Based upon the experience at Boulby better quality tents have been bought. These are mylar lined, which will help electromagnetic shielding, and are more effective at blocking light entering the tent. To further improve the light tightness a tailored cover is placed over the tent. In addition, the optical fibers are now placed inside a black tubing since laboratory tests have indicated that the fiber cover is not sufficient to block stray light entering the box. The rig mechanics is also being adjusted to provide a more diffuse and uniform illumination of the PMTs. Finally, the LED driver box has been adjusted to provide a lower level of illumination without the ND filter. All these changes, informed by the the experience in the tests of the pre-series at Boulby will lead to a setup that will allow to test the final series of PMTs. It is under consideration to exercise this setup to retest the pre-series PMTs.

References

[1] M. Askins et al. The Physics and Nuclear Nonproliferation Goals of WATCHMAN: A WAter CHerenkov Monitor for ANtineutrinos. *arXiv*, 2015.

[2] Hamamatsu. *Water-proof Type blah Photomultiplier Assembly R7081-100-10 WA-S80: Tentative Data Sheet*, December 2017.

[3] C. Bauer et al. Qualification Tests of 474 Photomultiplier Tubes for the Inner Detector of the Double Chooz Experiment. *JINST*, 6:P06008, 2011.

[4] G.D. Smith et al. WM-TN-002 WATCHMAN PMT Cable Tests.

[5] A. G. Wright. *The Photomultiplier Handbook*. Taylor and Francis, 2017.

[6] E. H. Bellamy et al. Absolute calibration and monitoring of a spectrometric channel using a photomultiplier. *Nucl. Instrum. Meth.*, A339:468–476, 1994.

[7] S-O Flyckt and C Marmonier. *Photomultiplier Tubes: Principles & Applications*. Photonis, September 2002.

[8] Photonis. Photomultiplier Tube Basics. www.photonis.com.

[9] A. Butcher et al. A method for characterizing after-pulsing and dark noise of PMTs and SiPMs. *Nucl. Instrum. Meth.*, A875:87–91, 2017.

[10] S. Aiello et al. Characterisation of the Hamamatsu photomultipliers for the KM3NeT Neutrino Telescope. *JINST*, 13(05):P05035, 2018.

[11] U. Akgun et al. Afterpulse timing and rate investigation of three different Hamamatsu photomultiplier tubes. *JINST*, 3:T01001, 2008.

[12] J. Haser et al. Afterpulse Measurements of R7081 Photomultipliers for the Double Chooz Experiment. *JINST*, 8:P04029, 2013.

Appendices

A Shipping Data

R7081-100-10 WA-S80 Shipping Data

	(1)	(2)	(3)	(4)	(5)	(6)	(7)	(8)	(9)
Serial No.	Sk (uA/lm)	Skb	Sp (A/lm)	Idb (nA)	EBB (V)	Dark Count (cps)	TTS (ns)	P/V	
NB0001	97	13.1	992	34	1500	2300	2.84	3.14	
NB0003	107	13.4	577	60	1650	3600	2.59	3.15	
NB0006	90	12.7	802	28	1530	2700	2.63	3.78	
NB0007	127	14.4	1070	60	1540	7700	3.13	2.69	
NB0009	102	13.7	560	100	1640	2900	3.06	3.18	
NB0010	120	14.0	712	320	1620	6800	2.76	4.43	
NB0012	77	12.5	130	1.5	1980	1100	2.31	3.00	
NB0014	99	13.4	394	140	1720	2300	2.57	4.00	
NB0026	103	13.5	225	10	1900	3600	2.37	4.50	
NB0027	101	13.4	151	14	1860	3000	2.21	3.92	
NB0028	122	14.1	469	39	1720	2100	2.49	4.38	
NB0029	97	13.2	384	40	1720	1900	2.33	4.00	
NB0030	89	12.6	176	2.6	1940	1400	2.38	3.70	
NB0031	113	13.6	257	14	1890	2100	2.40	3.71	
NB0032	104	13.8	784	150	1560	6500	2.71	3.00	
NB0033	97	13.6	414	42	1700	2400	2.56	4.14	
NB0034	103	13.2	536	24	1660	2700	2.71	3.45	
NB0037	109	13.5	454	68	1710	6900	2.65	3.78	
NB0039	94	12.9	410	35	1700	5200	2.67	4.00	
NB0042	94	12.6	164	9.7	1970	6400	2.49	3.57	
NB0043	109	13.5	231	17	1930	8400	2.48	2.69	
NB0047	102	13.4	688	280	1590	7900	2.61	3.71	
NB0048	112	13.1	482	87	1700	3000	2.98	3.33	
NB0049	115	13.9	999	240	1530	3000	3.04	4.17	
NB0050	95	13.3	828	28	1530	4000	2.58	4.43	
NB0051	110	13.3	1750	1500	1410	5300	3.31	2.91	
NB0053	101	13.7	623	55	1610	3800	2.69	3.29	
NB0054	112	14.1	645	52	1630	7300	2.67	4.12	
NB0055	119	14.2	465	140	1730	2100	2.57	3.33	
NB0056	103	13.6	481	140	1680	1500	2.69	3.00	
NB0057	97	13.2	385	18	1720	1200	2.47	4.57	
NB0059	99	13.4	747	44	1560	2700	2.84	3.00	
NB0061	117	14.1	751	25	1600	3000	2.17	3.56	
NB0063	83	12.5	315	5.9	1730	700	2.67	4.33	
NB0065	99	13.0	189	65	1930	6100	2.28	3.38	
NB0066	102	12.9	276	18	1820	1800	2.58	3.64	
NB0067	116	14.0	537	90	1690	1900	2.69	3.45	
NB0073	129	14.0	328	16	1840	3200	2.50	3.08	

Figure 24: Shipping Data for 101 PMTs tested, 1/3

NB0074	127	14.8	370	33	1820	2700	2.59	3.56	
NB0075	146	15.4	337	27	1880	2400	2.29	4.78	
NB0076	106	13.2	255	6.9	1860	1100	2.56	3.78	
NB0078	142	15.4	276	7.5	1950	2600	2.36	3.62	
NB0081	147	15.8	250	140	1970	2500	2.41	4.00	
NB0082	139	15.7	653	95	1680	2700	2.53	4.17	
NB0083	116	14.3	711	86	1610	1900	2.55	3.71	
NB0084	146	15.7	1300	300	1530	4200	2.73	2.60	
NB0087	131	14.9	416	60	1780	7900	2.54	3.18	
NB0088	130	15.5	948	39	1570	2300	2.70	3.40	
NB0090	132	14.3	946	360	1570	6500	2.88	3.45	U
NB0092	118	15.1	325	17	1830	2200	2.44	4.75	
NB0094	125	14.7	293	19	1870	2900	2.54	3.36	
NB0096	113	13.8	342	280	1800	3900	2.53	3.50	
NB0097	130	14.6	611	99	1680	1700	2.70	4.10	
NB0098	119	14.0	1020	230	1530	1800	2.96	4.57	
NB0099	137	15.5	512	150	1740	3700	2.66	4.75	
NB0102	120	14.7	607	50	1660	2300	2.67	4.11	
NB0103	109	14.7	445	22	1710	1600	2.57	3.90	
NB0104	117	14.1	723	170	1610	1500	2.79	3.57	
NB0105	113	14.7	751	52	1590	2300	2.76	4.57	
NB0106	139	15.4	1820	270	1440	4300	3.00	3.75	
NB0107	128	14.2	2740	160	1350	3900	3.22	4.25	
NB0108	120	14.2	1920	370	1410	2600	3.12	4.08	
NB0111	125	15.4	1680	1100	1440	6400	2.92	4.18	
NB0112	123	13.9	308	21	1850	1500	2.41	4.44	
NB0130	127	15.2	645	41	1660	1400	2.49	4.78	U
NB0131	122	14.8	1210	85	1500	2400	2.90	4.36	U
NB0132	123	15.5	2250	84	1380	1800	2.95	4.12	U
NB0133	130	15.1	4130	1200	1290	2300	3.22	3.82	U
NB0134	113	14.6	5390	1800	1230	2500	3.41	4.00	
NB0135	105	14.4	2400	81	1340	1100	3.12	4.44	
NB0136	124	15.3	1220	140	1500	2500	2.86	4.62	
NB0138	114	15.0	2900	190	1320	4700	3.15	3.67	
NB0139	139	15.7	1310	250	1510	2200	2.94	4.40	
NB0140	133	15.4	1220	88	1520	2200	2.85	3.77	
NB0141	125	15.1	1790	260	1430	3800	2.97	4.22	
NB0142	108	14.0	1310	41	1460	2500	3.14	4.12	
NB0143	110	14.3	3080	85	1310	1400	3.37	4.22	
NB0145	125	15.1	569	27	1690	1800	2.67	4.50	
NB0146	120	14.4	678	67	1630	2100	2.73	4.55	
NB0147	128	15.2	1360	24	1490	3100	3.07	4.88	
NB0148	116	14.9	3160	38	1310	2100	3.15	4.78	
NB0149	125	15.1	1160	42	1520	3300	2.75	4.50	
NB0150	128	15.2	5550	590	1240	4200	3.28	4.00	

Figure 25: Shipping Data for 101 PMTs tested, 2/3

NB0152	116	14.2	3550	230	1290	2000	3.19	4.86	
NB0153	126	14.9	4360	280	1270	4000	3.52	4.14	
NB0154	130	15.5	2250	27	1390	2700	3.05	4.40	
NB0155	132	14.7	1100	190	1540	5000	2.88	4.40	
NB0157	104	12.8	3530	1100	1270	1300	3.12	4.78	
NB0158	103	14.6	3360	230	1280	900	3.53	4.57	
NB0159	109	14.2	3650	310	1280	2000	3.39	4.00	U
NB0160	111	12.9	509	110	1680	1500	3.09	3.10	V
NB0161	112	14.1	2780	240	1320	2800	2.96	4.29	
NB0162	120	15.1	2610	44	1350	2200	3.05	4.30	
NB0163	119	15.0	1810	210	1410	1200	2.76	4.27	
NB0164	118	14.4	3640	150	1280	2700	3.59	4.43	
NB0165	113	14.6	2600	230	1340	1200	3.02	4.57	
NB0166	123	14.5	2360	760	1370	2300	3.16	4.30	U
NB0167	124	15.3	1060	54	1530	1700	2.78	3.92	
NB0169	118	14.4	1470	77	1450	2100	2.78	4.00	
NB0170	109	13.6	868	55	1550	2000	2.64	3.86	
NB0171	124	15.2	753	26	1610	2500	2.67	4.18	U

(3),(4) Overall supply voltage is 1500 V
(5) Voltage give a gain of 1E+07
(6),(7),(8) Overall supply voltage is EBB
(9) U Also tested underground
V Nominal HV altered to 1300 V

Figure 26: Shipping Data for 101 PMTs tested, 3/3

B HV Splitter

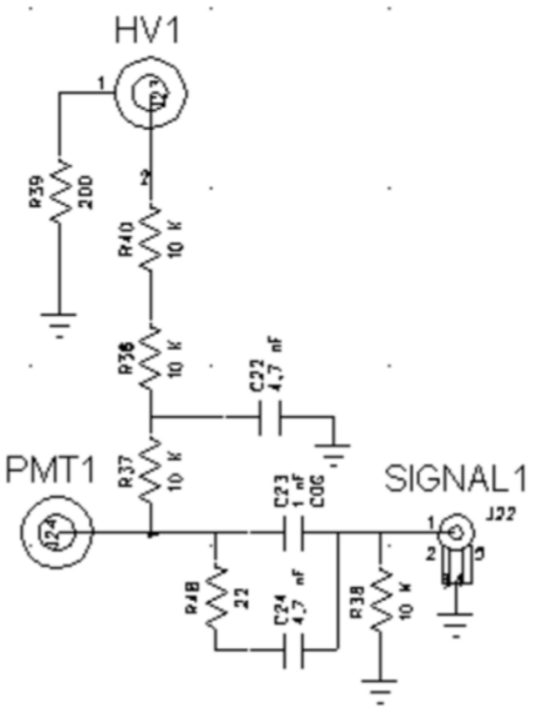

Figure 27: HV Splitter circuit diagram

C PMT Dynode Chain

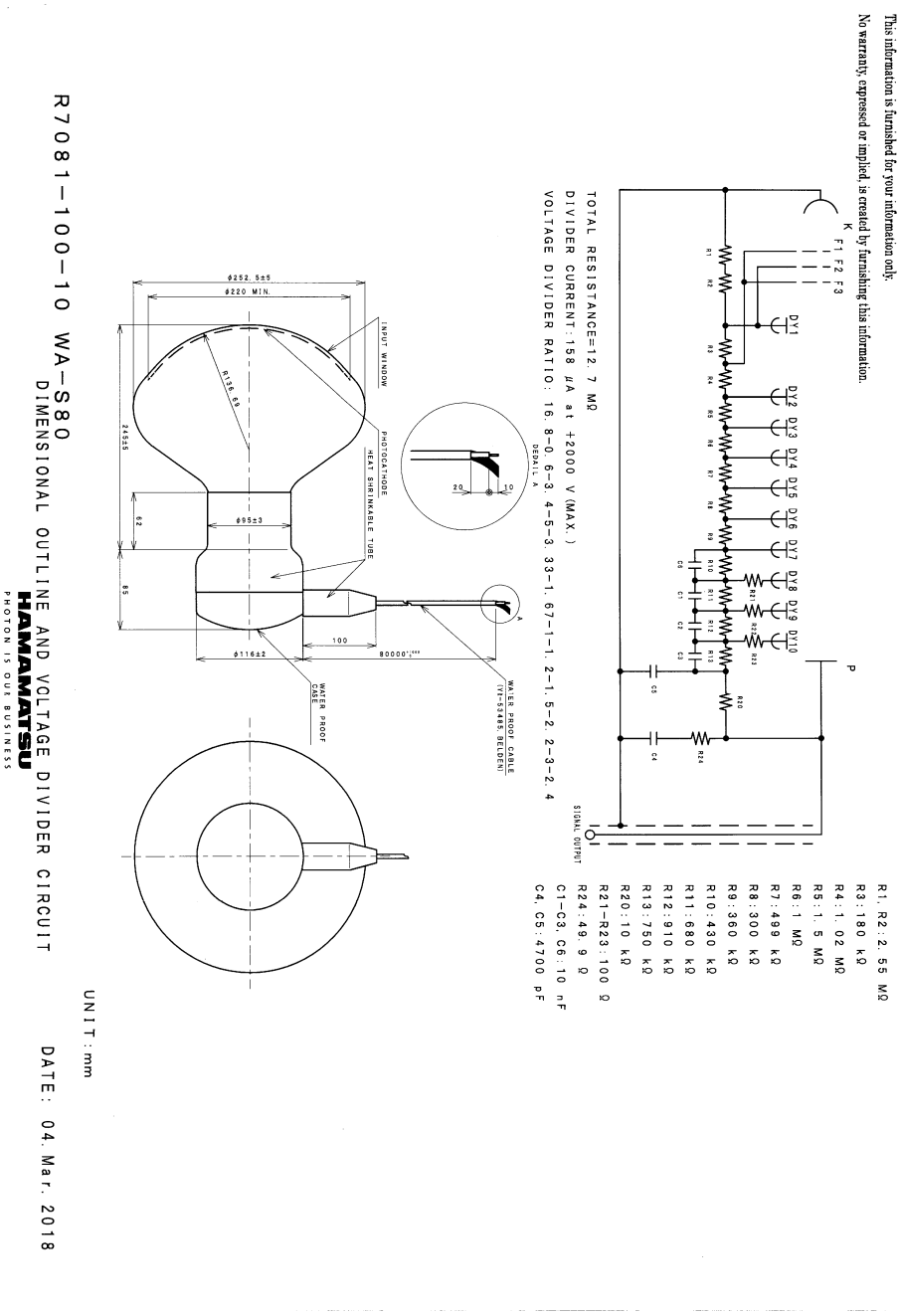

Figure 28: R7081 PMT dynode chain layout.